JOURNAL OF CATALYSIS 95, 120–136 (1985)

$NiMoO_4$ Selective Oxidation Catalysts Containing Excess MoO_3 for the Conversion of C_4 Hydrocarbons to Maleic Anhydride

I. Preparation and Characterization

U. OZKAN[1] AND G. L. SCHRADER[2]

Department of Chemical Engineering and Ames Laboratory—USDOE, Iowa State University, Ames, Iowa 50011

Received September 15, 1984; revised April 5, 1985

$NiMoO_4$ catalysts containing "excess" MoO_3 are active for the selective oxidation of C_4 hydrocarbons to maleic anhydride. The synthesis and characterization of the active component of this catalyst are reported. Synthesis techniques included precipitation, solid-state reaction, and impregnation. Extensive characterization of the catalyst has been performed using complementary instrumentation techniques, including laser Raman spectroscopy, Raman microprobe spectroscopy, X-ray diffraction, X-ray fluorescence, X-ray photoelectron spectroscopy, and scanning electron microscopy. © 1985 Academic Press, Inc.

1. INTRODUCTION

Simple molybdate compounds have been widely studied because of their catalytic activity for selective oxidation reactions, including ammoxidation and the oxidative dehydrogenation of olefins. An extensive body of literature has reported the characterization and catalytic evaluation of these compounds, especially bismuth and cobalt molybdates (*1–6*).

A more limited number of reports in the literature has revealed that pronounced changes in the catalytic behavior of simple molybdates can be observed due to the incorporation of "excess" MoO_3. The term "excess" MoO_3 is used to refer to the presence of MoO_3 in the catalyst, in addition to the simple molybdate itself; the molybdenum-to-metal stoichiometric ratio (e.g., Mo/Ni, Mo/Co, Mo/Bi) is therefore larger than the atomic ratio found in the pure, simple molybdates. In this respect, the catalysts which contain "excess" MoO_3 are no longer simple, one-phase oxides; rather, multiphase behavior—as well as other structural and compositional variations—are possible, making these catalysts much more complex than simple molybdates.

In two patents Hartig (*7, 8*) has reported the preparation of catalysts with nonstoichiometric atomic ratios of molybdenum-to-cobalt or molybdenum-to-nickel (compared to $CoMoO_4$ or $NiMoO_4$); the effect of preparation procedures on catalytic activity was also indicated. Appreciable yields of maleic anhydride were obtained from saturated aliphatics (C_4 to C_{10}) when cobalt or nickel molybdate catalysts with nonstoichiometric compositions were used. Matsuura *et al.* (*9*) have shown that bismuth molybdate catalysts with a molybdenum-to-bismuth ratio greater than that for γ-Bi_2MoO_6 are highly active for the oxidative dehydrogenation of butene to butadiene. Oganowski *et al.* (*10*) investigated the effect of excess MoO_3 on $MgMoO_4$ catalysts for the oxidative dehydrogenation of ethylbenzene to styrene. The presence of excess MoO_3 enhanced catalytic activity. It has also been shown by Grzybowska *et al.* (*11–13*) that the activity of cobalt molybdate for

[1] Present address: Department of Chemical Engineering, Ohio State University, Columbus, Ohio 43210.

[2] To whom correspondence should be addressed.

0021-9517/85 $3.00

the selective oxidation of propylene and allyl iodide to acrylic acid depends on the amount of excess MoO_3 present. Mazzocchia *et al.* (*14*) studied propylene oxidation over $NiO–MoO_3$ catalysts with Mo/Ni ratios greater or less than 1; only those catalysts with excess MoO_3 produced acrylic acid. They have also reported oxidation of 1-butene over the same catalysts (*15*).

Although strong evidence exists that the presence of MoO_3 is a key factor in determining the catalytic behavior of simple molybdate catalysts for selective oxidation, a fundamental understanding of the nature of these catalysts has yet to be developed. In this series of papers (*16–18*), we report the detailed synthesis and characterization of $NiMoO_4$ catalysts containing excess MoO_3 and also the corresponding relationship to catalytic activity and selectivity. Our results indicate that specific levels of MoO_3 concentration are required for high selectivity for 1-butene conversion to maleic anhydride; pure $NiMoO_4$ or MoO_3 are shown to be nonselective.

The previous paper in this series (*16*) has reported an investigation of the preparation procedures for the $NiMoO_4$ system. The present paper discusses methods for incorporating excess MoO_3 into the catalyst including precipitation, solid-state reaction, and impregnation. Extensive characterization of the catalysts has also been performed using complementary instrumentation techniques. The third paper (*17*) will provide activity and selectivity data for 1-butene conversion, while the fourth paper (*18*) will discuss the selective oxidation of butadiene and furan.

2. EXPERIMENTAL METHODS

2.A. *Catalyst Preparation*

2.A.1. Precipitation from aqueous solutions. Nickel molybdate catalysts were prepared from aqueous solutions of ammonium heptamolybdate (Fisher, $(NH_4)_6Mo_7O_{24} \cdot 7H_2O$) and nickel nitrate (Fisher, $Ni(NO_3)_2 \cdot 6H_2O$). The pHs of the solutions were varied by adding ammonium hydroxide or nitric acid. The procedure described by Schrader *et al.* (*16*) was adopted:

1. A 750-ml volume of a 0.4 *M* nickel nitrate solution was placed in a 2000-ml four-neck, round-bottom reaction vessel. The reaction mixture was heated to 60°C.

2. A 750-ml volume of a 0.0571 *M* ammonium heptamolybdate solution was added dropwise to the nickel nitrate solution. The solution was stirred vigorously during this period. The temperature was kept constant at 63°C using a temperature controller. The pH was controlled using a pH controller. Total time for addition was 0.5 h.

3. For preparation of pure nickel molybdate, the pH during addition and reaction periods was maintained at 6.

4. For preparations which involved incorporation of excess MoO_3, the precipitation medium was made more acidic during the addition period; the pH depended on the desired amount of excess MoO_3. The pH was raised to 5.5 at the end of the addition period and then was held constant.

5. After 4 h the precipitation mixture was filtered.

6. The precipitate was dried in air at 110°C for 12 h. Calcination under a steady flow of oxygen was performed at 500°C for 4 h.

2.A.2. Solid-state synthesis. Nickel molybdate samples were also synthesized by solid-state techniques which involved heating mixtures of nickel oxide (Fisher, NiO) and molybdenum trioxide (Fisher, MoO_3) in evacuated quartz tubes. Several reaction temperatures in the range of 700 to 1000°C were used.

Solid-state preparation was also an alternate method for incorporating excess MoO_3 into pure $NiMoO_4$ samples. Pure $NiMoO_4$ samples (synthesized by precipitation) and molybdenum trioxide (Fisher) were mechanically mixed in various ratios and were heated in dry oxygen at 500°C for 4 hours.

2.A.3. Impregnation of pure phases. For some studies pure $NiMoO_4$ samples (pre-

pared by precipitation) were impregnated with ammonium heptamolybdate to produce catalysts containing excess MoO_3. A 1.372×10^{-2} *M* ammonium heptamolybdate solution was prepared, and portions of nickel molybdate samples were immersed in this aqueous solution. The impregnation period was followed by drying at 110°C for 12 h and by calcining at 500°C under oxygen for 4 h. To achieve higher concentrations of excess MoO_3, a stepwise impregnation procedure was followed.

For impregnating molybdenum trioxide with $NiMoO_4$, an impregnation technique was used in which MoO_3 samples were soaked in an aqueous slurry of nickel molybdate. Samples were dried and calcined as described for the previous samples.

2.B. *Characterization Techniques*

2.B.1. Surface area. Surface areas were measured with a Micromeritics 2100E Accusorb. Nitrogen was used as the adsorbate.

2.B.2. X-Ray fluorescence. A Siemens SRS 200 sequential X-ray fluorescence spectrometer was used for compositional analysis. A Cr excitation source was used. Standards of varying compositions were prepared from mixtures of the oxides (NiO and MoO_3).

2.B.3. X-Ray diffraction. X-Ray powder diffraction patterns were obtained using a Picker θ-θ X-ray diffractometer automated by a PDP 15 computer system. Molybdenum K_α radiation was used. An internal standard (LiF) was used for alignment purposes. For some measurements a Siemens diffractometer having superior spatial resolution was employed with Cu K_α radiation. Samples were rotated in the X-ray beam. As an additional X-ray diffraction technique, an Enraf–Nonius Delft FR 552 Guinier camera was also used with Cu K_α radiation.

2.B.4. Laser Raman spectroscopy. Raman spectra were obtained using a Spex 1403 laser Raman spectrometer. Spectra were taken using the backscattering mode. The 514.3-nm line of a 4-W Spectra Physics argon ion laser was the primary excitation source. Approximately 200 mW of laser output at the source was used. A spectral resolution of 5 cm^{-1} and a central slit setting of 60 μm were maintained for all experiments. A Nicolet 1180E computer system was used for data acquisition including spectral accumulation. All spectra reported represent an accumulation of scans, in some cases up to 50 scans.

2.B.5. Raman microprobe spectroscopy. Raman microprobe experiments were conducted using a Spex 1482 Micromate illuminator. The instrument consists of a research-grade Zeiss microscope modified for spectroscopic investigations and grafted to the entrance slit of the Spex 1403 spectrometer. A TV camera and a monitor are included for viewing the sample, so that the laser beam can be finely aligned and focused. Two standard objectives—a 10×, 0.22 numerical aperture objective or a 40×, 0.95 numerical aperture objective—could be used to focus the laser beam to a diameter of 5 or 2 μm, respectively.

Spectral parameters for the microprobe were the same as those for the conventional spectrometer studies except for the necessity of acquiring more (typically up to 100) scans.

2.B.6. X-Ray photoelectron spectroscopy. X-Ray photoelectron spectra were obtained using an AEI 200B spectrometer with Al K_α radiation. A Nicolet 1180 computer was used for data acquisition and for signal averaging. All spectra are referenced to the carbon 1*s* binding energy of 284.6 eV.

2.B.7. Scanning electron microscopy. Scanning electron microscopy studies were conducted using a JEOL Model JSM-U3 scanning electron microscope. Samples were prepared by sprinkling powder on the surface of a sample mount which had been covered with wet carbon black. The sample was then sputtered with gold to achieve a gold thickness of 300 Å. Micrographs were typically taken using a potential difference of 25 kV and a working distance of 13 mm.

TABLE 1

Stoichiometry of Precipitated $NiMoO_4$ Samples as a Function of pH as Established by X-Ray Fluorescence and Their Surface Areas

pH during addition period	pH during precipitation and aging periods	Mo/Ni	Surface area (m^2/g)
6	6	1.00	37
5	5.5	1.15	33
4	5.5	1.40	26
3	5.5	1.55	20
MoO_3			3

The electron microscope was also equipped with a Tracor/Northern 2000 energy dispersive X-ray microanalyzer. The microanalyzer was used for elemental mapping, single-line scanning, and X-ray spectral accumulation. Samples were prepared by silver sputtering rather than by gold sputtering to prevent interference with molybdenum radiation.

3. EXPERIMENTAL RESULTS

3.A. General Catalyst Preparation Parameters

The precipitation experiments for the Ni MoO_4 system indicated that the overall composition of the precipitated catalyst was insensitive to the concentration and composition of the reactants; the pH of the precipitation medium was the key factor which determined the amount of MoO_3 present in the final form of the catalyst (*16*). Pure $NiMoO_4$ catalysts were obtained at a pH of 6 and a temperature of 63°C, both conditions being maintained throughout the addition and precipitation periods. Lowering the pH of the reaction medium during addition resulted in the presence of MoO_3 in the final calcined samples.

For preparing catalysts with nonstoichiometric Mo/Ni ratios, solid-state and impregnation techniques were also successful. Using the impregnation technique, samples were synthesized having a wide concentration range of excess MoO_3—from 2 to 55%.

3.B. X-Ray Fluorescence

Precipitated samples were analyzed by X-ray fluorescence using calibration curves obtained from NiO and MoO_3 standards. The analysis indicated that a decrease in pH during addition resulted in an increase in the Mo/Ni ratio (Table 1).

3.C. Surface Area

Surface area measurements for the precipitated samples demonstrated that the composition of the catalysts strongly affected the catalyst surface area (Table 1). The surface area of pure $NiMoO_4$ is much larger compared to that of pure MoO_3 (37 vs 3 m^2/g), and the surface area of the catalysts decreased with increasing percentages of excess MoO_3.

3.D. X-Ray Diffraction

The X-ray diffraction pattern *d*-spacings of calcined samples prepared by precipitation at a pH of 6 correspond to those reported by Sleight and Chamberland (*19*) for α-$NiMoO_4$. The X-ray diffraction patterns of such samples also have no indication of the presence of MoO_3, NiO, or any other oxide.

Figure 1 shows a comparison of the X-ray diffraction patterns for pure MoO_3 (spectrum a), a $NiMoO_4$ sample prepared at a pH 5 during addition (spectrum b), a Ni MoO_4 sample containing 15% excess MoO_3 which was prepared by calcining mixtures of MoO_3 and $NiMoO_4$ at 500°C (spectrum c), and a $NiMoO_4$ sample prepared at a constant pH of 6 throughout addition and precipitation periods (spectrum d). For the powder pattern of the sample prepared at the more acidic condition, there are "extra" peaks which do not appear in the powder pattern of pure $NiMoO_4$. A comparison of the *d*-spacings indicate that these extra peaks correspond to MoO_3 (*20*). The same observation holds for the diffraction pattern of the sample prepared by solid-state reaction. All *d*-spacings in this pattern are assignable either to MoO_3 or $NiMoO_4$.

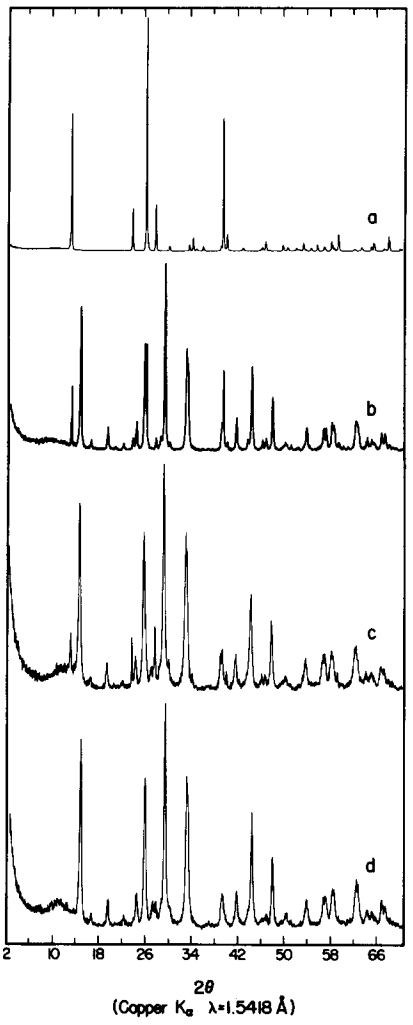

FIG. 1. Comparison of X-ray diffraction patterns for (a) pure MoO_3, (b) $NiMoO_4$ with excess MoO_3 (precipitation), (c) $NiMoO_4$ with excess MoO_3 (solid state), (d) pure $NiMoO_4$.

Table 2 shows the results obtained by Guinier camera measurements for a Ni MoO_4 sample prepared at a pH of 5 during addition. The *d*-spacings obtained for this sample correspond to the values reported in the literature for α-$NiMoO_4$ and MoO_3.

3.E. Laser Raman Spectroscopy

Raman spectroscopic characterization of $NiMoO_4$ during various stages of preparation by precipitation have been reported previously (*16*). In this paper emphasis is placed on the final state of catalysts containing MoO_3. Raman spectroscopy is a particularly powerful technique for detecting small amounts of MoO_3—at concentrations which are not detectable by X-ray diffraction. In addition, the Raman technique can be used to identify changes in crystallographic structure or deviations from "ideal" or anticipated material states.

Raman spectra of $NiMoO_4$ samples containing excess MoO_3 (prepared by precipitation, solid-state synthesis, and impregnation) are compared with those of pure MoO_3 and pure $NiMoO_4$ in Fig. 2. Comparison of the five spectra show that samples with nonstoichiometric Mo/Ni ratios have Raman bands characteristic of either Ni MoO_4 or MoO_3. There are no indications of the appearance of any extra bands or the shifting of bands. Table 3 lists the band positions for MoO_3, $NiMoO_4$, and a $NiMoO_4$ sample with excess MoO_3.

Figure 3 provides the Raman spectra of precipitated $NiMoO_4$ samples prepared at pH values of 3, 4, 5, and 6 during addition (spectra a, b, c, and d, respectively). Figure 3d is the spectrum of pure $NiMoO_4$. The other spectra exhibit more intense MoO_3

TABLE 2

d-Spacings Obtained by a Guinier Camera From a $NiMoO_4$ Sample Prepared at a pH of 5 during Addition

d-Spacing (Å)	Compound identification	*d*-Spacing (Å)	Compound identification
6.19	α-$NiMoO_4$	2.12	MoO_3
5.50	α-$NiMoO_4$	2.09	α-$NiMoO_4$
4.66	α-$NiMoO_4$	2.06	α-$NiMoO_4$
4.08	α-$NiMoO_4$	1.99	MoO_3
3.81	MoO_3	1.98	α-$NiMoO_4$, MoO_3
3.71	α-$NiMoO_4$	1.96	α-$NiMoO_4$, MoO_3
3.51	α-$NiMoO_4$	1.92	α-$NiMoO_4$
3.26	MoO_3	1.85	MoO_3
3.09	α-$NiMoO_4$	1.83	α-$NiMoO_4$
2.75	α-$NiMoO_4$	1.80	α-$NiMoO_4$
2.72	α-$NiMoO_4$	1.73	MoO_3
2.70	MoO_3	1.72	α-$NiMoO_4$
2.65	MoO_3	1.66	MoO_3
2.33	α-$NiMoO_4$	1.64	α-$NiMoO_4$
2.32	α-$NiMoO_4$, MoO_3	1.62	α-$NiMoO_4$
2.30	α-$NiMoO_4$	1.60	α-$NiMoO_4$, MoO_3
2.19	α-$NiMoO_4$		

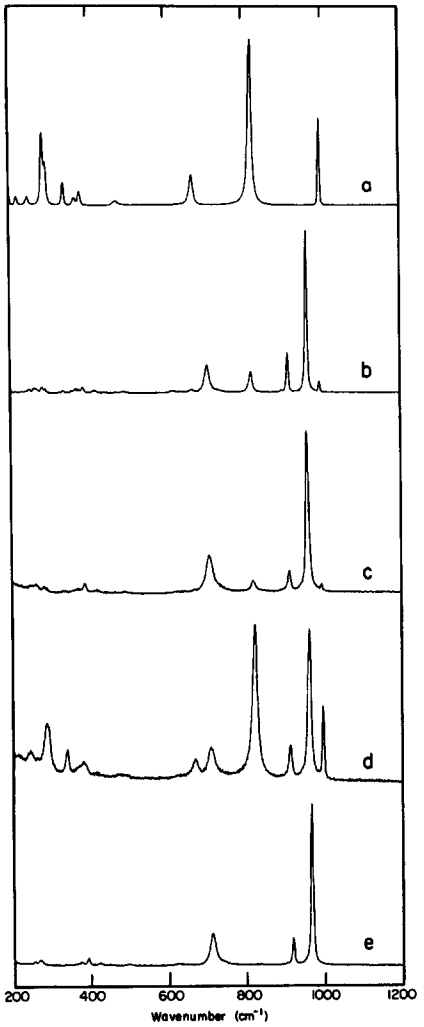

FIG. 2. Raman spectra of (a) pure MoO_3, (b) $NiMoO_4$ with excess MoO_3 (precipitation), (c) $NiMoO_4$ with excess MoO_3 (solid state), (d) $NiMoO_4$ with excess MoO_3 (impregnation), (e) pure $NiMoO_4$.

bands as the acidity of the precipitation medium increases. This is in excellent agreement with the results obtained by X-ray fluorescence analysis.

Detailed Raman characterization studies have also been carried out in the low-wavenumber region (50–350 cm^{-1}) for some of the precipitated samples containing excess MoO_3. The lattice phonon region of the Raman spectrum can reflect deviations from "ideal" or expected crystal structure. Figure 4 shows the low-wavenumber Raman spectra of pure MoO_3 (a), pure $NiMoO_4$ (c), and $NiMoO_4$ with 15% excess MoO_3 prepared by precipitation (b). No unexpected spectral features were observed.

In order to investigate the effect of preparation procedure on the active form of the catalyst, Raman characterization experiments have also been performed for impregnated MoO_3 samples. Figure 5 shows the Raman spectrum of such a sample. It is seen that bands corresponding to both MoO_3 and $NiMoO_4$ (although weak) are present without any band shifts for either phase.

3.F. Raman Microprobe Spectroscopy

This technique with its superior spatial resolution allows the laser beam to be fo-

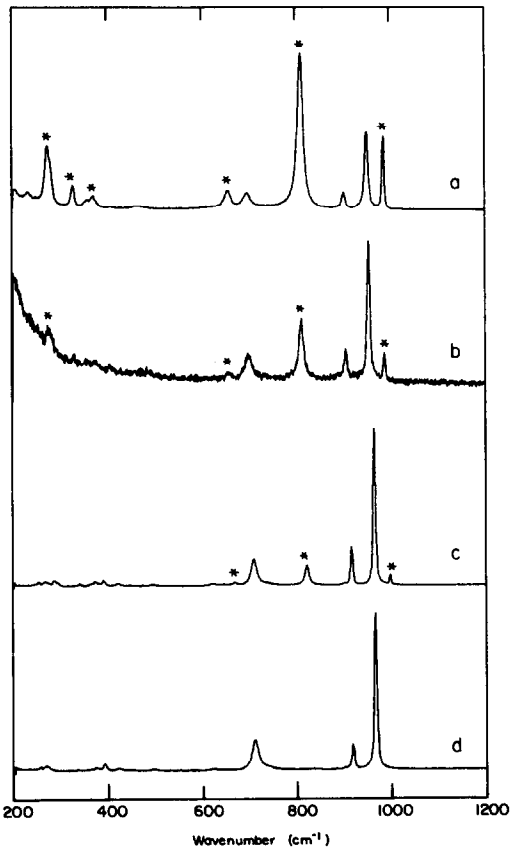

FIG. 3. Raman spectra of precipitated $NiMoO_4$ samples. (a) pH 3, (b) pH 4, (c) pH 5, (d) pH 6. Asterisk indicates MoO_3.

TABLE 3

Raman Bands of MoO_3, $NiMoO_4$, and Catalyst with "Excess" MoO_3

Sample	(cm^{-1})					
	0–200	200–400	400–600	600–800	800–1000	1000+
MoO_3	85 m	219 w	475 w	670 s	822 vs	
	100 w	247 w			998 s	
	118 m	285 s				
	131 m	293 m				
	160 m	339 m				
	200 w	369 w				
		381 m				
$NiMoO_4$	55 w	229 vw	420 m	623 w	833 vw	
	143 w	254 w	445 w	642 vw	916 s	
	179 m	264 w	494 m	709 s	963 vs	
	196 w	301 vw				
	374 w	331 w				
	389 m	373 m				
		389 m				
$NiMoO_4$ with 15% excess MoO_3 (precipitation)	55 w	219 w	420 m	620 m	821 s	
	99 vw	230 vw	464 w	642 w	916 s	
	117 m	253 w	475 vw	668 m	963 vs	
	130 w	264 m	494 m	709 s	997 s	
	114 w	285 s				
	158 m	293 m				
	179 m	331 w				
	199 m	339 m				
		373 m				
		379 w				
		389 m				

cused on individual particles while viewing the magnified image on a monitor. This capability when combined with the SEM studies made it possible to differentiate two crystallite shapes, one irregular and roundish and the other hexagonal. Based on the two-dimensional outlines observed, the former image was associated with $NiMoO_4$ and the latter with MoO_3.

Figure 6 shows two spectra obtained

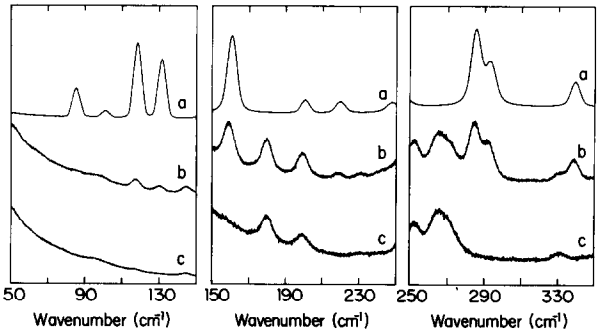

FIG. 4. Low-wavenumber Raman spectra of (a) pure MoO_3, (b) $NiMoO_4$ with excess MoO_3 (precipitation), (c) pure $NiMoO_4$.

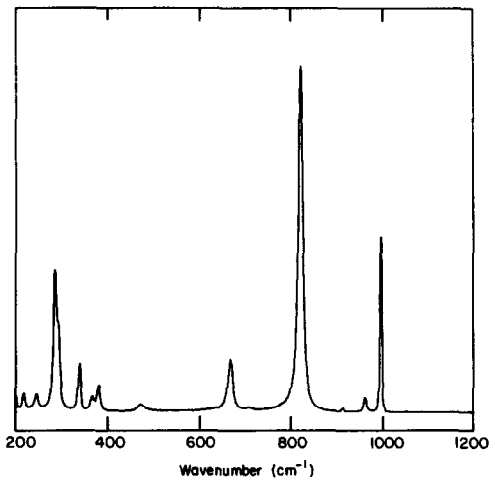

FIG. 5. Raman spectrum of impregnated MoO_3.

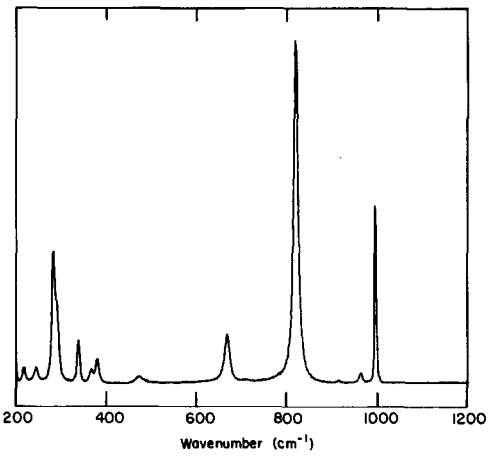

FIG. 7. Raman microprobe spectrum of impregnated MoO_3.

from the same sample—an impregnated Ni MoO_4 catalyst containing 10% excess MoO_3. In the bottom spectrum (b), the laser beam is focused on a roundish particle, and the Raman spectrum is comprised of Ni MoO_4 bands only. The second spectrum was obtained by focusing the laser beam on a particle which has an apparent MoO_3 crystallite shape; the major bands of both $NiMoO_4$ and MoO_3 are present. Raman microprobe results present the most compelling evidence that separate phases are present in these catalysts. Furthermore, the microprobe results indicate that particles which have typical shape of MoO_3 crystallites contain not only MoO_3 but also Ni MoO_4 as well.

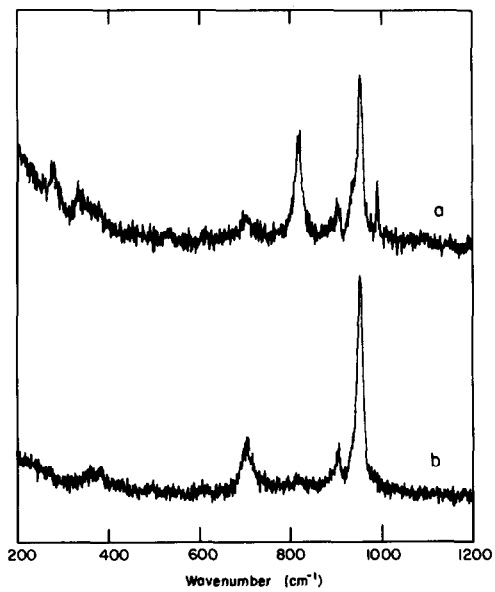

FIG. 6. Raman microprobe spectra of impregnated $NiMoO_4$. Laser beam focused on (a) a hexagonal particle and (b) a round particle.

The spectra obtained from impregnated MoO_3 samples also indicate the presence of $NiMoO_4$ on the surface of individual MoO_3 particles (Fig. 7).

The Raman microprobe experiments also revealed that a polymolybdate layer did not exist on the surface of $NiMoO_4$. Such surface phases have been observed for alumina-supported molybdate samples (*21*). However, there is an unambiguous absence of Raman bands in the region which would be used to identify this structure.

3.G. X-Ray Photoelectron Spectroscopy

X-Ray photoelectron spectra were acquired in order to investigate possible variations in the oxidation states of samples with nonstoichiometric compositions. Figure 8 shows the molybdenum 3*d* photoelectron spectra of pure MoO_3 (a), pure Ni MoO_4 (b), and two $NiMoO_4$ samples containing excess MoO_3 (c and d) which

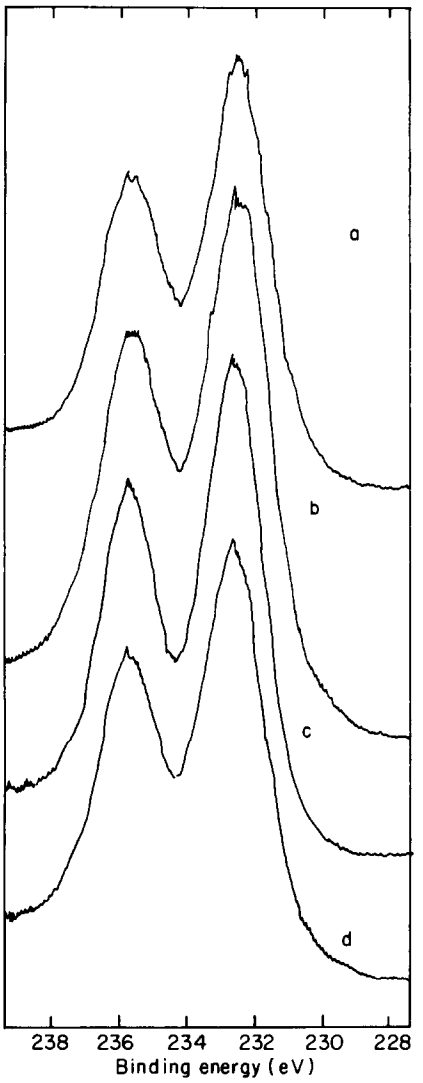

FIG. 8. Molybdenum 3*d* photoelectron spectra of (a) MoO_3, (b) $NiMoO_4$, (c) $NiMoO_4$ with excess MoO_3 (precipitation), (d) $NiMoO_4$ with excess MoO_3 (impregnation).

were prepared by different techniques. A comparison of the spectrum demonstrates that the band positions and the bandwidths are identical for these samples. Figure 9 shows the nickel 2*p* photoelectron spectra for the same samples.

Table 4 lists the observed binding energies (±0.2 eV) for the samples mentioned above. The band positions for MoO_3 agree very well with those reported in the literature (*22*). The Mo 3*d* binding energies for $NiMoO_4$ samples are identical with those of MoO_3. The Ni 2*p* band positions, on the other hand, are entirely different than those of NiO (*22*).

3.H. Scanning Electron Microscopy

Scanning electron microscopy studies contributed significantly to the development of a better understanding of the nature of the active form of complex $NiMoO_4$ catalysts. The technique can provide information about the morphological structure of surfaces and about elemental composition with the use of energy dispersive X-ray analysis.

Figures 10 and 11 show scanning electron micrographs of two $NiMoO_4$ precursors. The first sample (Fig. 10), prepared at a pH of 6, ultimately produced pure $NiMoO_4$ upon calcination. The second sample (Fig. 11) is a precursor prepared at a pH of 3 which gave rise to a nonstoichiometric Mo/Ni ratio in the final form of the catalyst. When the micrographs are compared, it is

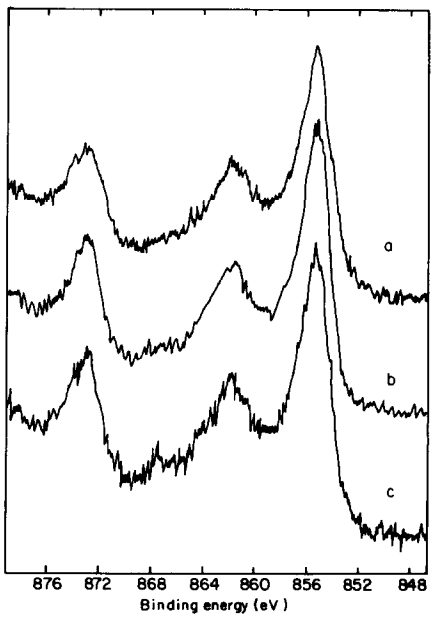

FIG. 9. Nickel 2*p* photoelectron spectra of (a) $NiMoO_4$, (b) $NiMoO_4$ with excess MoO_3 (precipitation), (c) $NiMoO_4$ with excess MoO_3 (impregnation).

TABLE 4

Photoelectron Spectra Binding Energies for Pure Compounds and Catalysts (eV)

Sample	Mo $3d_{5/2}$	Mo $3d_{3/2}$	Ni $2p_{3/2}$	Ni $2p_{1/2}$
MoO_3	232.7	235.8		
MoO_3 (*22*)	232.65	235.85		
$NiMoO_4$	232.6	235.7	855.7	873.3
NiO (*22*)			853.3	871.7
$NiMoO_4$ with 15% excess MoO_3 (precipitation)	232.7	235.8	855.8	873.4
$NiMoO_4$ with 15% excess MoO_3 (impregnation)	232.7	235.9	855.7	873.4

seen that the latter preparation contains a second type of particle shape (a, upper right corner) which did not appear in the micrographs in Fig. 10. Figure 11b is a close-up of the same specific particle, which is believed to correspond to the precursor of MoO_3.

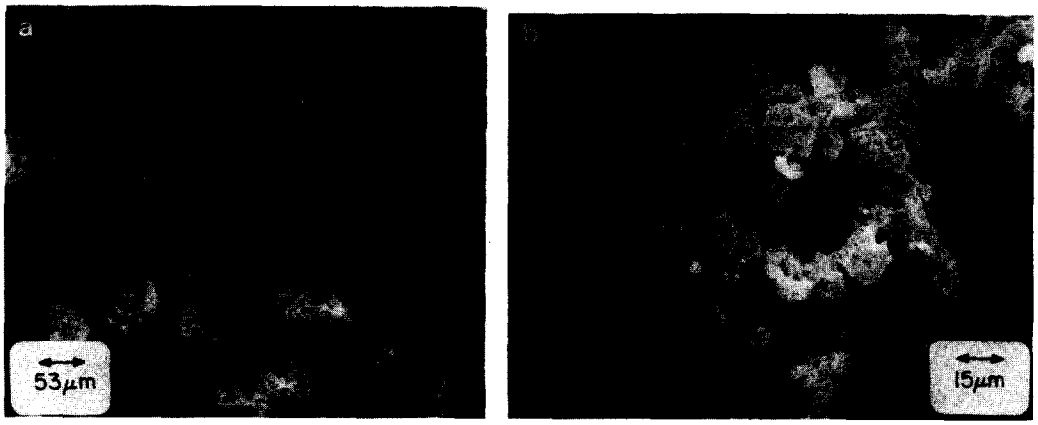

FIG. 10. Scanning electron micrographs of $NiMoO_4$ precursor prepared at pH 6. Magnification: (a) 190× and (b) 680×.

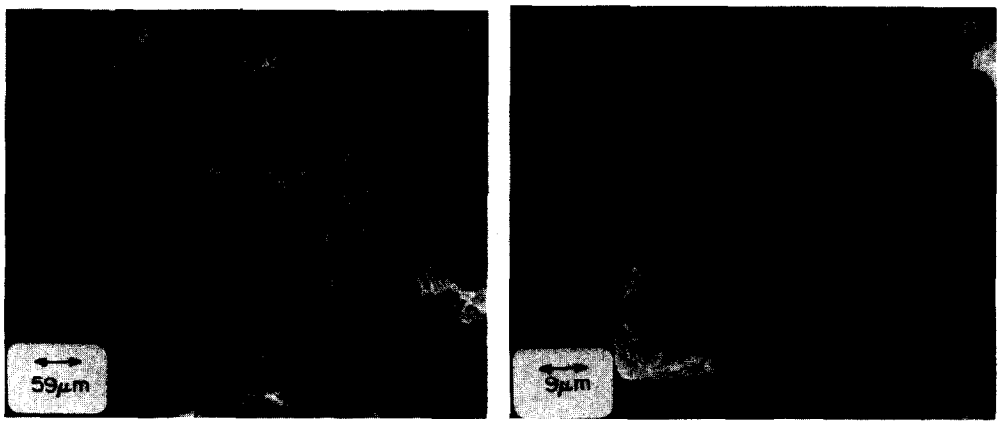

FIG. 11. Scanning electron micrographs of $NiMoO_4$ precursor prepared at pH 3. Magnification (a) 170× and (b) 1134×.

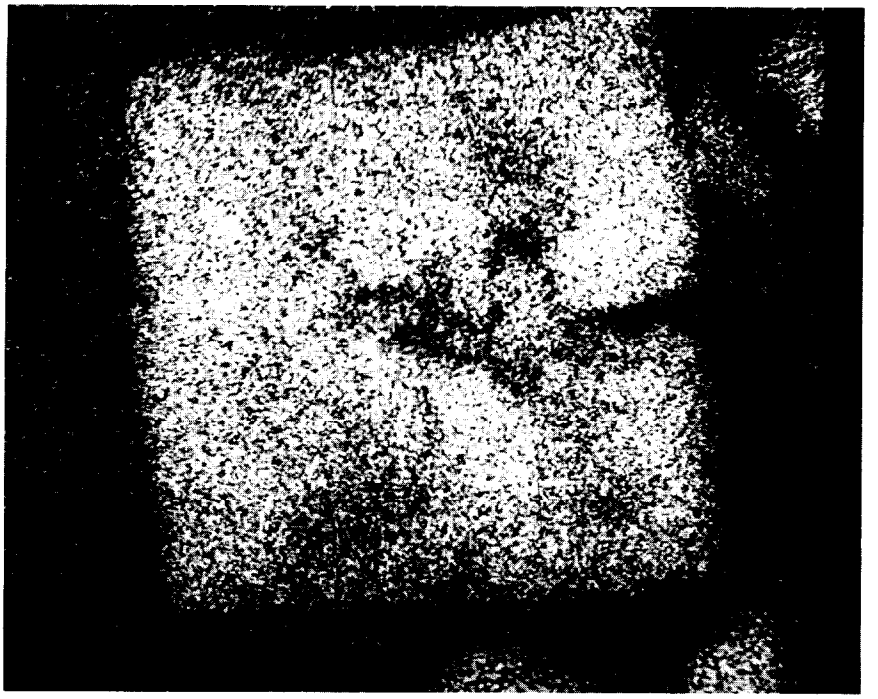

FIG. 12. Elemental map for molybdenum.

Figure 12 shows the elemental map on this particle for molybdenum L_α radiation. A high Mo concentration was detected.

Figure 13 compares the crystallite shapes of pure MoO_3 (a) and pure $NiMoO_4$ (b). MoO_3 crystallites have definite, well-defined hexagonal shapes which are easily recognized. On the other hand, $NiMoO_4$ consists of porous, roundish particles having a "sponge-like" structure.

When catalysts with nonstoichiometric Mo/Ni ratios were studied using SEM, their two-phase character became apparent once more. Figure 14 shows two micrographs taken from a precipitated sample containing excess MoO_3. Separate $NiMoO_4$ and MoO_3

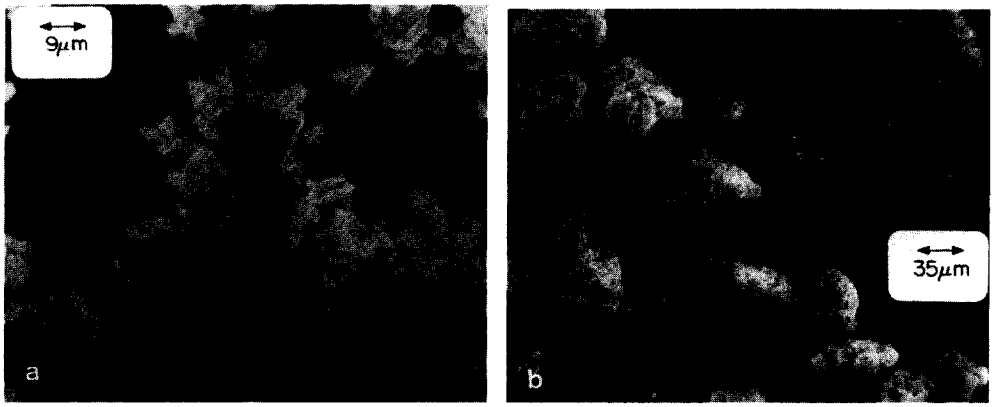

FIG. 13. Scanning electron micrographs of (a) pure MoO_3, magnification = 1134× and (b) pure $NiMoO_4$, magnification = 283×.

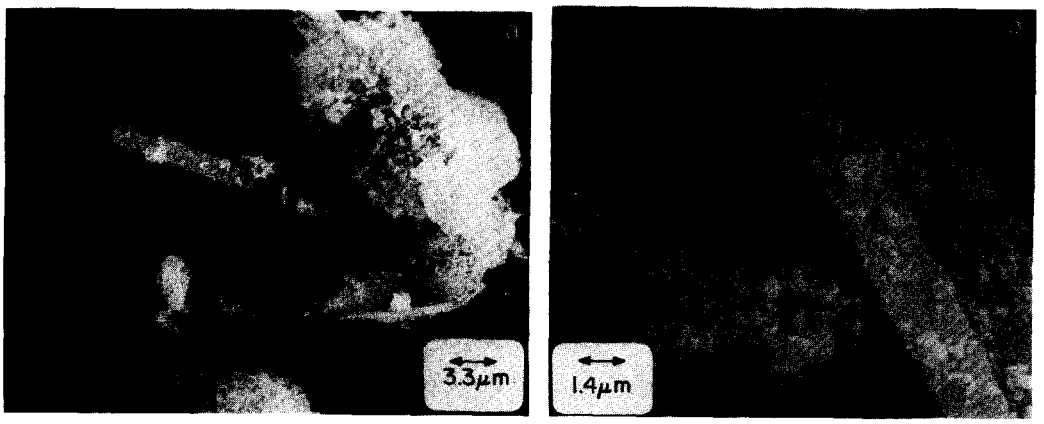

FIG. 14. Scanning electron micrographs of $NiMoO_4$ catalyst with excess MoO_3 (precipitation). Magnification (a) 2980× and (b) 7228×.

particles can be easily identified. An important feature of these micrographs is that surface of MoO_3 particles is not flat and smooth as it is for pure MoO_3; rather it is cluttered or decorated with $NiMoO_4$. When the X-ray microanalyzer technique was used to examine these samples, the existence of $NiMoO_4$ on the MoO_3 particles was confirmed. Figure 15 shows two X-ray spectra showing the relative intensities of the Mo and Ni signals obtained for a pure $NiMoO_4$ particle (a) and for a MoO_3 particle (b) present in a "nonstoichiometric" preparation. The signal intensity ratio of molybdenum compared to nickel is much larger for the sample shown in Fig. 15b since Ni MoO_4 exists only as a surface coverage and the bulk of the particle is MoO_3.

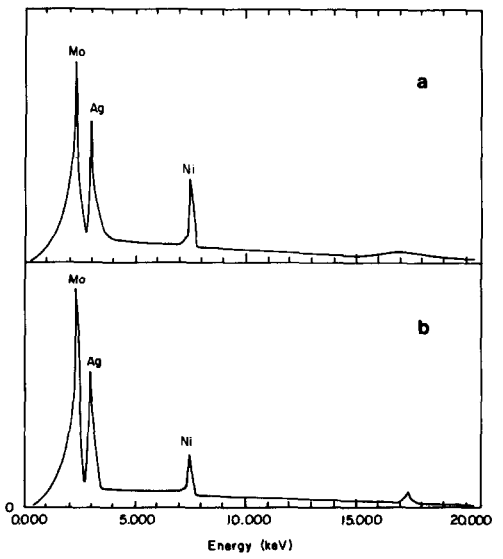

FIG. 15. X-Ray spectra of (a) pure $NiMoO_4$ and (b) MoO_3 particle found in a $NiMoO_4$ catalyst with excess MoO_3.

The same phenomenon is also observed in the samples prepared by the solid-state technique. Distinct $NiMoO_4$ and MoO_3 particles (with a surface coverage) are seen. Figures 16 and 17 show four micrographs which were taken from a sample prepared by solid-state methods.

The impregnation technique also provided further evidence for the coexistence of two distinct phases—a $NiMoO_4$ phase and a MoO_3 phase with an additional surface structure. Figure 18 shows two micrographs taken from the same sample which was prepared by impregnation of $NiMoO_4$. The sample contains 10% excess MoO_3. In Fig. 18a both $NiMoO_4$ and MoO_3 particles can be observed. In Fig. 18b, the typical shape of the MoO_3 crystallite is very distinctive, although the surface is cluttered.

When impregnated $NiMoO_4$ samples having the two extremes in the concentration of excess MoO_3 (2 and 55%) were examined by SEM, two new phenomena were

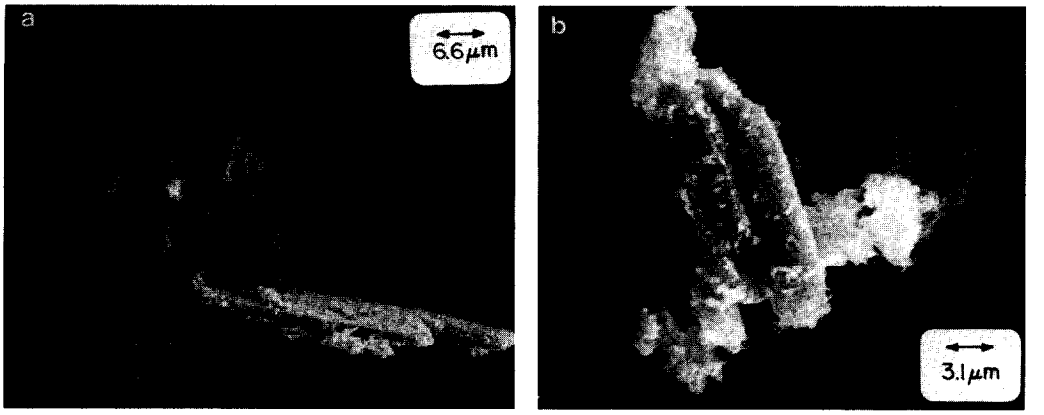

FIG. 16. Scanning electron micrographs of $NiMoO_4$ with excess MoO_3 (solid state). Magnification: (a) 1506× and (b) 3210×.

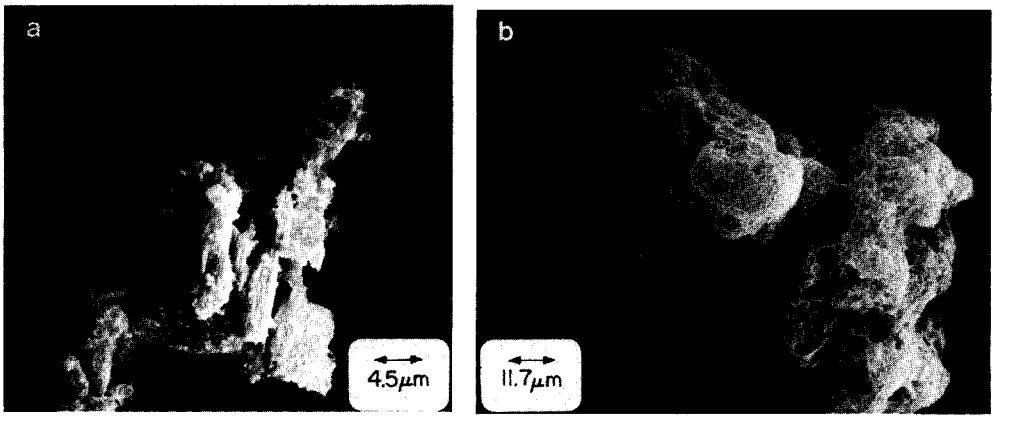

FIG. 17. Scanning electron micrographs of $NiMoO_4$ with excess MoO_3 (solid state). Magnification: (a) 2200× and (b) 850×.

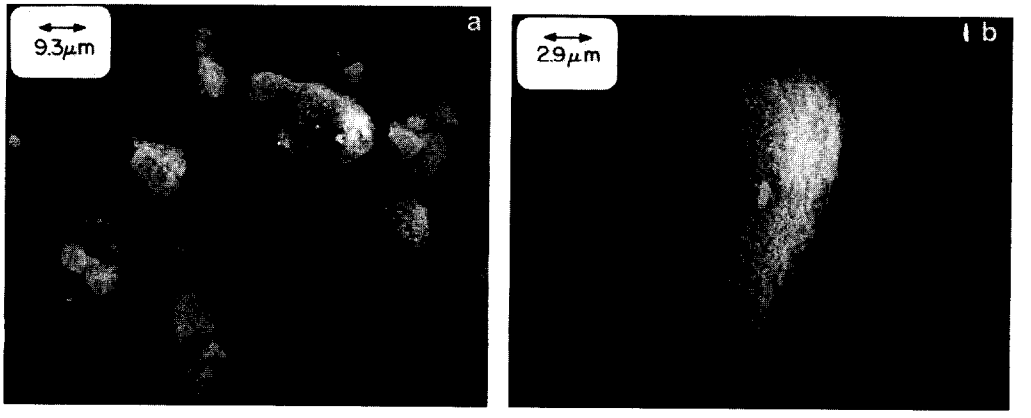

FIG. 18. Scanning electron micrographs of impregnated $NiMoO_4$ (10% excess MoO_3). Magnification: (a) 1077× and (b) 3440×.

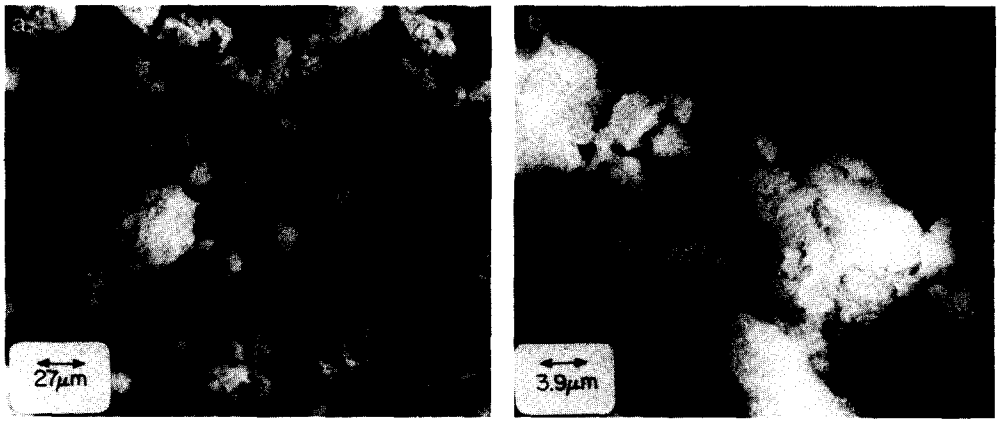

FIG. 19. Scanning electron micrographs of impregnated $NiMoO_4$ (2% excess MoO_3). Magnification: (a) 363× and (b) 2550×.

observed. The low MoO_3 concentration end showed no indication of the presence of MoO_3 as a separate phase. Although several samples were scanned repeatedly, no MoO_3 particle was observed as a distinct phase (Fig. 19). When the high MoO_3 concentration samples were characterized with SEM, it was found that separate MoO_3 clusters had formed at this concentration level. It was also noted that these clusters housed free MoO_3 particles which had no surface coverage of $NiMoO_4$ (Fig. 20).

Impregnated MoO_3 samples were also characterized with SEM. Figure 21, which was taken from a sample which contained 15% excess $NiMoO_4$, shows that the surfaces of the MoO_3 crystals are cluttered with $NiMoO_4$.

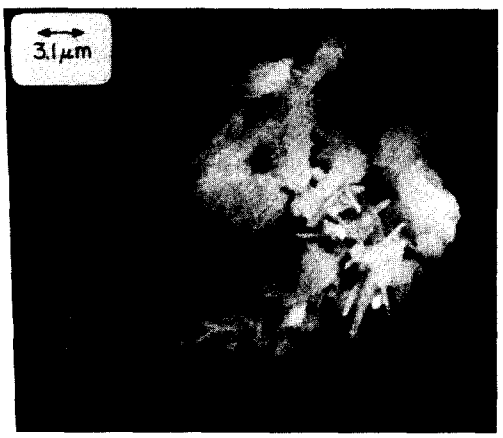

FIG. 20. Scanning electron micrograph of impregnated $NiMoO_4$ (55% excess MoO_3). Magnification = 3210×.

4. DISCUSSION OF RESULTS

The multiphase nature of the catalytic system necessitated the use of combination of complementary characterization techniques in order to acquire a fundamental understanding of the structural and compositional characteristics of the catalyst. X-Ray diffraction and Raman spectroscopy verify that there are no impurities present in precipitated samples prepared at a pH of 6. Raman spectroscopy (both conventional and microprobe techniques) provides very reliable evidence for the absence of MoO_3 in this sample since MoO_3 is an excellent Raman scatterer. When these two techniques are combined with X-ray fluorescence analyses, the compositions of the precipitated catalysts can be determined with a high degree of certainty. Preparation of rigorously pure $NiMoO_4$ (as established by several complementary techniques) was essential for the activity measurements performed in these studies. Only if pure Ni MoO_4 samples were available could the crucial importance of excess MoO_3 be established.

In samples which were prepared at pH

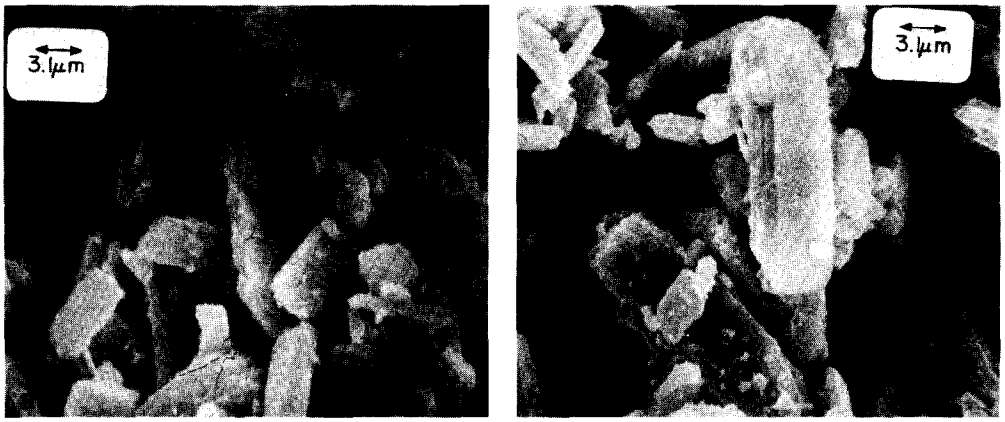

FIG. 21. Scanning electron micrographs of impregnated MoO_3. Magnification (a) 3210× and (b) 3210×.

values lower than 6, both $NiMoO_4$ and MoO_3 have been clearly shown to be present (Figs. 1 and 2). It has also been shown using X-ray fluorescence that the Mo/Ni ratio increases with decreasing pH of the precipitation medium (Table 1). The effect of pH on aqueous molybdenum species has been discussed elsewhere (*16*). The results of X-ray fluorescence analysis have been further verified by the detection of MoO_3 using Raman spectroscopy (Fig. 3). In this respect, this work differs significantly from that of Grimblot *et al.* (*23*) who report that for samples with molar ratios Mo/Ni > 1, only MoO_3 was detected. Since no indication of the final compositional analysis of their samples has been provided, it is not possible to draw any conclusions as to why $NiMoO_4$ could not be detected in their samples. Raman spectroscopic characterization experiments have shown that solid-state and impregnation techniques also can be used to incorporate excess MoO_3 (Fig. 2).

In order to investigate if there is a change in the lattice parameters of $NiMoO_4$ due to the presence of excess MoO_3, diffraction patterns of samples with nonstoichiometric compositions were acquired using a Guinier camera (Table 2). The results show that the lattice structure of $NiMoO_4$ remains unchanged by the presence of excess MoO_3. The Raman spectroscopy measurements were also carried out in the low-wavenumber region to investigate perturbation of lattice phonon bands; the Raman evidence supported the X-ray results (Fig. 7), although the Raman information would not probably be conclusive without the Guinier camera experiments.

X-Ray photoelectron spectroscopy provides further insight into the nature of these catalysts. The molybdenum 3*d* binding energies for MoO_3 agree very well with those found in the literature (*22*). The Ni $2p_{3/2}$ binding energy for $NiMoO_4$ also agrees very closely with that reported by Grimblot *et al.* (*23*) for pure α-$NiMoO_4$ (Table 4). Comparison of the molybdenum 3*d* photoelectron spectra for MoO_3, $NiMoO_4$, and $NiMoO_4$ samples with nonstoichiometric Mo/Ni ratios show that the spectra are virtually identical. This is important in demonstrating that the oxidation state of molybdenum does not change in these samples (Fig. 8). The same observation is true for a comparison of the nickel 2*p* photoelectron spectra in pure $NiMoO_4$ and in two $NiMoO_4$ samples with Mo/Ni ratios larger than 1.0 (Fig. 9). The pronounced difference which exists between the nickel 2*p* binding energies of $NiMoO_4$ and NiO also clearly establishes that there is no NiO present in any samples (Table 4). Since the oxidation states and the

structural coordination of both Mo and Ni are unaffected by the presence of excess MoO_3, the possibility of having an entirely new, unanticipated compound formed by the various preparation procedures is eliminated.

Having thus established the presence of both MoO_3 and $NiMoO_4$ phases in the excess MoO_3 samples, it was then determined using scanning electron microscopy that these catalysts exhibited a distinct-particle identity. The scanning electron micrographs taken on these samples exhibited two different types of particles which were easily identified as MoO_3 and $NiMoO_4$ crystallites (Fig. 14). The distinct-particle character of these samples was quite apparent in several other excess molybdenum samples, regardless of the preparation technique used (Figs. 16–18). In addition to the observation of these distinct phases, it was also observed in these micrographs that the surfaces of MoO_3 particles were covered with a porous material which closely resembled $NiMoO_4$. When energy-dispersive X-ray spectrum was taken on a MoO_3 particle which had such a surface layer, the spectrum clearly showed the presence of nickel on the particle (Fig. 15b). The ratio of the Mo signal to the Ni signal was greater than the ratio obtained from the X-ray spectrum of a pure $NiMoO_4$ particle (Fig. 15a), since the $NiMoO_4$ was only covering the surface of the MoO_3 crystallite.

Raman microprobe experiments provided further confirmation of this same specific particle state and association. This technique, with its excellent spatial resolution, provided both compositional and structural spectroscopic information about specific areas of the sample; the magnified visual images of the sample were also helpful. It was possible to distinguish between the $NiMoO_4$ particles and the primarily MoO_3 particles. Figure 6 shows two spectra taken from the same sample. In Fig. 6b, the laser beam was focused on a particle which had the obvious characteristics of $NiMoO_4$. In the other spectrum (Fig. 6a), the beam was focused on a hexagonal particle which clearly resembled MoO_3. The pronounced difference between the two spectra shows not only that the two types of particles detected by SEM are structurally different but also that they have different compositions. In addition to the evidence presented by energy-dispersive X-ray microanalysis that nickel is present on the MoO_3 particles (Fig. 15b), the Raman microprobe results clearly show that the small particles adhering to the particle surface are identifiable as $NiMoO_4$ with respect to composition and structure (Fig. 6a). The same state of the catalyst was also observed for impregnated catalysts. The electron micrographs show a typical $NiMoO_4$ structure covering the surface of the MoO_3 particles (Fig. 21), and Raman microprobe results identified this phase as $NiMoO_4$ (Fig. 7).

5. CONCLUSIONS

Selective oxidation catalysts typically consist of a mixture of metal oxides which are prepared by precipitation techniques. The nature of the final calcined state of these catalysts is complex, and a strong dependence on preparation procedures is usually exhibited. For the conversion of 1-butene to maleic anhydride using $NiMoO_4$-based catalysts, this study has indicated that the structural and compositional properties of the catalysts must be examined in considerable detail using several complementary instrumentation techniques.

The synthesis and characterization experiments reported here in general reveal the potential complexity of metal oxide selective oxidation catalysts. Several possible compositional and structural states must be considered. Formation of a solid solution of metal oxides is possible: however, neither precipitation nor solid-state synthesis were shown by X-ray diffraction and Raman spectroscopy to produce such behavior for $NiMoO_4$. Similarly, no new compound formation was detected with any of the complementary techniques; only $NiMoO_4$ and

MoO_3 were present in the samples. Formation of a homogeneous dispersion of the phases is also a possibility for complex mixed metal oxides. Raman microprobe and SEM investigations are powerful methods for examining the particulate structure of catalyst powders. In this study, distinct crystallites of $NiMoO_4$ and MoO_3 have been observed to exist. However, these investigations have also indicated that a specific state of association of the particles is crucial: the surfaces of MoO_3 crystallites were covered with $NiMoO_4$ particles. Alternative structures—such as a monolayer coverage of polymolybdates on $NiMoO_4$ or an association of MoO_3 crystallites on the Ni MoO_4 surface—were shown not to exist.

As a result of this detailed synthesis and characterization, catalytic selectivity can be related to a specific state of the metal oxide system. This relationship is established in the next papers in this series.

ACKNOWLEDGMENTS

This work was conducted through the Ames Laboratory which is operated for the U.S. Department of Energy by Iowa State University under Contract W-7405-ENG-82. The X-ray photoelectron spectroscopy work by James W. Anderegg and Guinier camera X-ray diffraction experiments by Bernd U. Harbrecht are gratefully acknowledged.

REFERENCES

1. Batist, Ph. A., Kapteijns, C. J., Lippens, B. D., and Schuit, G. C. A., *J. Catal.* **7,** 33 (1967).
2. Batist, Ph. A., Prette, H. J., and Schuit, G. C. A., *J. Catal.* **15,** 267 (1969).
3. Haber, J., *J. Less-Common Met.* **36,** 277 (1974).
4. Trifirò, F., Caputo, G., and Villa, P. L., *J. Less-Common Met.* **36,** 305 (1974).
5. Burrington, J. D., and Grasselli, R. K., *J. Catal.* **59,** 79 (1979).
6. Burrington, J. D., Kartisek, C. T., and Grasselli, R. K., *J. Catal.* **63,** 235 (1980).
7. Hartig, M. J. D., U.S. Patent 2,625,519; Jan. 13, 1953.
8. Hartig, M. J. D., U.S. Patent 2,691,600; Oct. 12, 1954.
9. Matsuura, I., Schut, R., and Hirakana, K., *J. Catal.* **63,** 152 (1980).
10. Oganowski, W., Hanuza, J., Jezowska-Trzebiatowska, B., and Wrzyszcz, J., *J. Catal.* **39,** 161 (1975).
11. Grzybowska, B., and Mazurkiewicz, A., *Bull. Acad. Pol. Sci., Ser. Sci. Chem.* **27**(2), 141 (1979).
12. Grzybowska, B., and Mazurkiewicz, A., *Bull. Acad. Pol. Sci., Ser. Sci. Chem.* **27**(2), 149 (1979).
13. Grzybowska, B., Haber, J., and Janas, J., *J. Catal.* **49,** 150 (1977).
14. Mazzocchia, C., Di Renzo, F., Centola, P., and Del Rosso, R., *in* "Proceedings, 4th International Conference on the Chemistry and Uses of Molybdenum." Climax Molybdenum Co., Golden, Colo., 1982.
15. Mazzocchia, C., Del Rosso, R., and Centola, P., *in* "Proceedings, 5th Ibero-American Symposium on Catalysis." Lisbon, Portugal, 1979.
16. Schrader, G. L., Sivrioglu, U., and Basista, M. A., *in* "Proceedings, 4th International Conference on the Chemistry and Uses of Molybdenum." Climax Molybdenum Co., Golden, Colo., 1982.
17. Ozkan, U., and Schrader, G. L., *J. Catal.* **95,** 137 (1985).
18. Ozkan, U., and Schrader, G. L., *J. Catal.* **95,** 147 (1985).
19. Sleight, A. W., and Chamberland, B. L., *Inorg. Chem.* **78**(8), 1672 (1980).
20. Kihlborg, L., *Acta Chem. Scand.* **13,** 954 (1959).
21. Cheng, C. P., and Schrader, G. L., *J. Catal.* **60,** 276 (1979).
22. Wagner, C. D., Riggs, W. M., Davis, L. E., Moulder, J. F., and Muilerberg, C. E., "Handbook of X-Ray Photoelectron Spectroscopy." Perkin–Elmer Corp., Minnesota, 1978.
23. Grimblot, J., Payen, E., and Bonnelle, J. P., *in* "Proceedings, 4th International Conference on the Chemistry and Uses of Molybdenum." Climax Molybdenum Co., Golden, Colo., 1982.